Inorganica Chimica Acta 362 (2009) 1448–1454

Contents lists available at ScienceDirect

Inorganica Chimica Acta

journal homepage: www.elsevier.com/locate/ica

Synthesis, crystal structure and photoelectric property of Mn(II/IV) coordination complexes

Li Zhang [a], Shu-Yun Niu [a,*], Jing Jin [a], Li-Ping Sun [a], Guang-Di Yang [b], Ling Ye [b]

[a] *School of Chemistry and Chemical Engineering, Liaoning Normal University, Huanghe Road, Dalian 116029, PR China*
[b] *Key Laboratory of Supramolecular Structure and Materials of Ministry of Education, Jilin University, Changchun 130023, PR China*

ARTICLE INFO

Article history:
Received 11 March 2008
Received in revised form 3 July 2008
Accepted 9 July 2008
Available online 15 July 2008

Keywords:
Manganese (II/IV)
Coordination complex
Synthesis
Crystal structure
Surface photovoltage

ABSTRACT

Three novel coordination complexes $[Mn(tpha)(phen)]_n$ (**1**); $[Mn(na)_2(H_2O)_2]_n$ (**2**); $\{[Mn(phen)_2(OH)Cl] \cdot Cl \cdot (OH) \cdot (C_9H_{11}NO_2) \cdot 2H_2O\}$ (**3**) have been hydrothermally synthesized and structurally characterized by single-crystal X-ray diffraction (H_2tpha = terephthalic acid, Hna = nicotinic acid, phen = 1,10-phenanthroline). The tpha groups in complex **1** bridge the Mn(II) ions to an infinite 3D framework. Complex **2** exhibits a 2D network structure in which the Mn(II) ions are linked by nicotinic groups. Complex **3** is connected to a 2D coordination supramolecule by hydrogen bonds. The results of surface photovoltage spectra (SPS) of complexes **1–3** indicate that they all exhibit positive surface photovoltage (SPV) responses in the range of 300–800 nm. However, the intensity, position and numbers of SPV responses are obviously different. The distinctions can be mainly attributed to their structures, valences and coordination environments of the manganese ions in the three complexes. Moreover the external field induced surface photovoltage spectra (FISPS) of the three complexes have been measured.

1. Introduction

Manganese ions play important roles in biological redox systems. They are necessary for glucose and fat oxidation processes as well as other basic biochemistry functions [1–5]. Because the valences of manganese ions are rich and the electronic structures are diverse, manganese complexes with different oxidation states, configurations and dimensions have been widely focused by researchers [6–10]. The extensive studies of manganese coordination complexes indicate that they possess potential applications in molecular magnet, medicine synthesis, biochemistry, catalysis and many other domains [11–16].

The energy gaps of some transitional metal polymers are sometimes in the region of the gaps of semiconductors. This phenomenon means that they can show certain semiconductor characteristic and therefore be considered as some type of inorganic–organic hybrid semiconductors. The detection about surface charge behaviors and photoelectric properties of transitional metal coordination polymers will provide special references for further research on the functions of these complexes. At present, the researches about this aspect have been mainly focused on compounds with porphyrins and phthalocyanines as ligands, however, there are few reports on coordination polymers [17,18].

The surface photovoltage spectroscopy (SPS) technique, a very sensitive characterization method which detects the change of charge distribution on a solid material surface, is not only related to the electron transition process caused by light absorption but also directly reflects the property of photogenerated charge separation and charge transfer [19–21]. At present, this technique has been successfully employed for the study of the charge transfer in photo-stimulated surface interactions, dye sensitization processes, photo-catalysis and the process of charge transition between solid materials surfaces and phases [22–25]. Based on the SPS, Wang et al. have developed an external field induced surface photovoltage technique [26,27], which can demonstrate the photoelectric property of solid material surface under the effect of an external electric field. In this paper, we report the syntheses, crystal structures and surface photoelectric properties of three Mn(II/IV) coordination complexes. Furthermore we compare and analyze the influences of different structures, valences and coordination environments on photoelectric properties of the complexes.

2. Experimental

2.1. Materials and apparatus

All reagents were of A.R. grade. Infrared (IR) spectra were recorded on a JASCO FT-IR/480 Spectrophotometer in the range of

---

[*] Corresponding author. Fax: +86 411 82156832.
E-mail address: syniu@sohu.com (S.-Y. Niu).

0020-1693/$ - see front matter © 2008 Elsevier B.V. All rights reserved.
doi:10.1016/j.ica.2008.07.010

220–4000 cm^{-1} using KBr pellets. UV–Vis spectra were obtained on a JASCO UV/Vis/NIR UV-570 Spectrophotometer in the range of 200–800 nm using solid powder. The elemental analysis of the complexes was determined by a PE-240C Analyzer and a PLASAM-SPEC-II instrument. SPS and FISPS measurements were conducted with the light source-monochromator-lock-in detection technique. All the measurements were performed under atmospheric pressure at ambient temperature.

2.2. Synthesis of complexes 1, 2 and 3

$[Mn(tpha)(phen)]_n$ (**1**): A solution of $MnCl_2 \cdot 4H_2O$ (0.19 g, 0.96 mmol) in water (10 mL) was added to an ethanol solution (10 mL) of H_2tpha (0.17 g, 0.97 mmol), and then phen (0.05 g, 0.97 mmol) was added into the above solution. The color of the solution turned yellow. The mixture was then transferred into a Teflon-lined stainless steel vessel that was sealed and heated to 170 °C for 5 days. Having been cooled to room temperature, yellow crystals of complex **1** were collected. Yield: 0.260 g (67.9%) *Anal.* Calc. for $C_{20}H_{12}N_2O_4Mn$: C, 60.17; H, 3.03; N, 7.02; Mn, 13.76. Found: C, 59.85; H, 2.91; N, 7.10; Mn, 13.35%. IR data (KBr pellet, cm^{-1}): 3441 (ν_{-OH}); 3062 (ν_{Ar-H}); 1597 ($\nu_{as-coo-}$); 1385 (ν_{s-coo-}); 1513, 1495, 1425 ($\nu_{C\cdots C}$); 845, 806 ($_{Ar-H}$); 750 (ν_{Mn-O}); 505 (ν_{Mn-N}).

$[Mn(na)_2(H_2O)_2]_n$ (**2**): A solution of $MnCl_2 \cdot 4H_2O$ (0.19 g, 0.96 mmol) in water (10 mL) was added to a solution of nicotinic acid (0.12 g, 1.0 mmol) and NaOH (0.04 g, 1.00 mmol) in water (10 mL). The solution was colorless. Then the mixture was transferred into a Teflon-lined stainless steel vessel, and the vessel was sealed and heated to 170 °C for 5 days. Having been cooled to room temperature, colorless crystals of complex **2** were collected. Yield: 0.126 g (39.2%). *Anal.* Calc. for $C_{12}H_{12}N_2O_6Mn$: C, 43.00; H, 3.61; N, 8.36; Mn, 16.39. Found: C, 42.20; H, 3.48; N, 8.54; Mn, 16.11%. IR data (KBr pellet, cm^{-1}): 3306 (ν_{-OH}); 3043 (ν_{Ar-H}); 1612 ($\nu_{as-coo-}$); 1393(ν_{s-coo-}); 1594, 1563, 1427 ($\nu_{C\cdots C}$); 1197 ($_{-OH}$); 1160, 1045 ($\nu_{C-N,\ C-O}$); 862, 755, 701 ($_{Ar-H}$); 555 (ν_{Mn-O}); 419(ν_{Mn-N}).

$[Mn(phen)_2(OH)Cl] \cdot Cl \cdot OH \cdot 2H_2O \cdot C_9H_{11}NO_2$ (**3**): A solution of $MnCl_2 \cdot 4H_2O$ (0.19 g, 0.96 mmol) in water (10 mL) was added to a solution of 4-aminobenzoic acid (0.15 g, 1.09 mmol) and NaOH (0.04 g, 1.00 mmol) in water (10 mL), and then phen (0.05 g, 0.97 mmol) and ethanol solution (5 mL) was added into the above solution. The color of the solution turned red. The mixture was transferred into a Teflon-lined stainless steel vessel that was sealed and heated to 170 °C for 5 days. Having been cooled to room temperature, red crystals of complex **3** were collected. Yield: 0.296 g (42.8%). *Anal.* Calc. for $C_{33}H_{33}N_5Cl_2O_6Mn$: C, 54.94; H, 4.61; N, 9.71; Mn, 7.61. Found: C, 54.37; H, 4.35; N, 9.89; Mn, 7.39%. IR data (KBr pellet, cm^{-1}): 3563 (ν_{-NH}); 3050 (ν_{Ar-H}); 2994, 2929, 2609 (ν_{-OH}, ν_{-NH}); 1620 ($\nu_{as-coo-}$); 1424 (ν_{s-coo-}); 1589, 1572, 1514, 1492 ($\nu_{C\cdots C}$); 1221 ($_{-OH}$); 1141, 1100, (ν_{C-N}, ν_{C-O}); 860, 728 ($_{Ar-H}$); 637 (ν_{Mn-O}); 418 (ν_{Mn-N}); 276 (ν_{Mn-Cl}).

2.3. Determination of crystal structure

Crystallographic data for complexes **1** and **2** were collected on a Rigaku R-AXIS-RAPID diffractometer using graphite monochromated Mo Kα radiation (λ = 0.71073 Å) at 293 K. Crystallographic data for complex **3** was collected on a Smart APEX II CCD diffractometer using graphite monochromated Mo Kα radiation (λ = 0.71073 Å) at 293 K. All data were corrected for Lorentz polarization factor and empirical absorption. The structures were solved by direct method and refined by full matrix least-squares calculations on F^2 using SHELXTL 97 program. The crystal data and structure refinement of complexes **1–3** are summarized in Table 1.

Table 1
Summary of data collections and structure refinements for complexes **1, 2** and **3**

	1	**2**	**3**
Empirical formula	$C_{20}H_{12}N_2MnO_4$	$C_{12}H_{12}N_2MnO_6$	$C_{33}H_{33}N_5Cl_2MnO_6$
Formula weight	399.26	335.18	721.48
Temperature (K)	293(2)	293(2)	293(2)
Crystal system	monoclinic	monoclinic	triclinic
Space group	$C2/c$	$P2(1)/c$	$P\bar{1}$
a (Å)	17.436(7)	8.7340(17)	11.130(4)
b (Å)	10.313(5)	10.182(2)	11.517(4)
c (Å)	9.294(6)	7.1369(14)	14.803(5)
α (°)	90	90	70.401(5)
β (°)	96.18(2)	99.98(3)	85.326(5)
γ (°)	90	90	72.829(5)
V (Å^3)	1661.6(16)	625.1(2)	1707.5(11)
Z	4	2	2
D_{calc} (g cm^{-3})	1.596	1.781	1.403
F(000)	812	342	746
Goodness-of-fit on F^2	1.077	1.086	1.023
Reflections collected/unique	7972/1895	5973/1429	10768/7880
Data/restraints/parameters	1895/0/123	1429/0/97	7880/0/516
Final R indices [$I > 2\sigma(I)$]	R_1 = 0.0304, wR_2 = 0.0730	R_1 = 0.0388, wR_2 = 0.1056	R_1 = 0.0608, wR_2 = 0.1304
R indices (all data)	R_1 = 0.0382, wR_2 = 0.0759	R_1 = 0.0429, wR_2 = 0.1083	R_1 = 0.1177, wR_2 = 0.1595
Largest difference peak and hole (e Å^{-3})	0.314 and −0.276	1.220 and −0.735	0.457 and −0.431

3. Results and discussion

3.1. Structural description of complexes 1, 2 and 3

The single-crystal X-ray diffraction analysis revealed that complex **1** exhibits a 3D infinite framework structure. The unit coordination is defined by four O atoms from four different tpha groups and two N atoms from one phen ligand around the Mn(II) ion in a distorted octahedronal fashion (Fig. 1). The bond length of Mn–N is 2.3440(18) Å and the distances of Mn–O are 2.1145(14) Å and 2.1369(15) Å, respectively. All the tpha groups can be separated into two categories (A and B) according to their space positions. The phenyl rings of the A kind (or B kind) are coplanar, while the phenyl rings between the A kind and B kind are twisted by 67.2°.

In crystal, tpha groups of A kind use four carboxylic O atoms to coordinate four different Mn(II) ions, which in turn are joined to a 1D chain along the *a*-axis direction. Along *c*-axis, tpha groups of B kind coordinate two adjacent Mn(II) ions through two carboxylic O atoms by a bidentate bridging mode which makes the Mn(II) ions connect to a 2D structure in *ac* layer (Fig. 2). Between the two 2D layers, the other carboxylic O atoms of B kind tpha groups adopt the same mode to link adjacent Mn(II) ions (Fig. 3). Therefore, Mn(II) ions are further connected to a 3D infinite structure (Supplementary Fig. 1s). When projected along *c*-axis, it can be seen clearly that the layers cross each other and form many regular lozenge holes. All the phen molecules arrange regularly in the lozenge holes (Fig. 4). The regular structure is beneficial for transferring electrons or holes.

Complex **2** possesses a 2D infinite structure and its building unit is $[Mn(na)_2(H_2O)_2]$. Each Mn(II) ion is six coordinated. Two N atoms and two O atoms are from four different nicotinic groups, and two O atoms are from two coordinated water molecules. The coordination environment of Mn(II) ion is a slightly distorted octahedron (Fig. 5). The bond lengths of Mn–O range from 2.1632(17) Å to 2.1835(17) Å and Mn–N are 2.2860(19) Å. O1 and O1C, O3 and O3C, N1A and N1D are all centro-symmetric for Mn(II) ion. One N atom and one carboxylic O atom from the nicotinic group coordinate two different

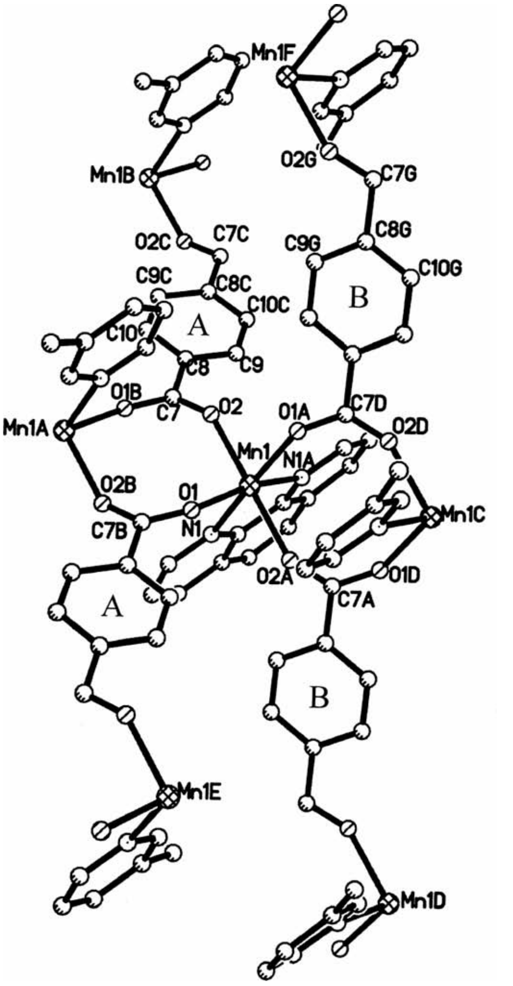

Fig. 1. Coordination environment of Mn(II) ion in complex **1**.

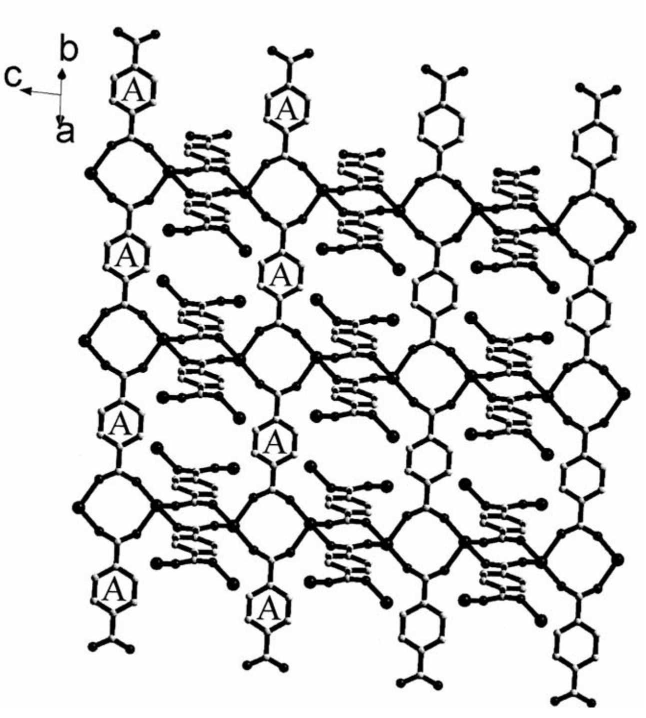

Fig. 2. *ac* layer of complex **1** (Phen molecules are omitted for clarity).

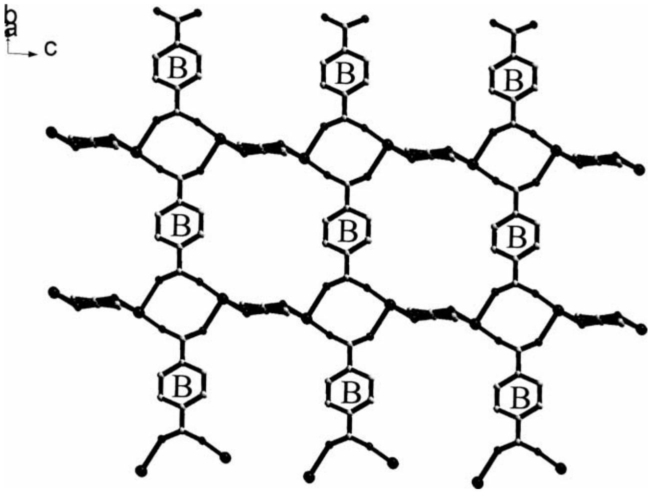

Fig. 3. *bc* layer of complex **1** (Phen molecules are omitted for clarity).

Mn(II) ions, and then the Mn(II) ions are connected to a 1D zigzag chain along *b*-axis (Supplementary Fig. 2s). Nicotinic groups link Mn(II) ions in adjacent chains by the same mode as described above, which makes the Mn(II) ions link another 1D chain along *c*-axis. Therefore, complex **2** is further connected to a 2D infinite structure in *bc* plane (Fig. 6).

Complex **3** is an ionic complex. The molecular structure is given in Fig. 7. In cation, the six coordination atoms of Mn(IV) are from two phen molecules, one hydroxyl and a chlorine anion. One chlorine anion, one hydroxyl, two free water molecules and one 4-aminobenzoate consist of the outside environment. Since none of 4-aminobenzoate was added to the starting reaction mixture, we speculate that it may be the result of reaction between 4-aminobenzoic acid and ethanol.

In crystal, water molecules, hydroxyl, chlorine anions and N atoms of 4-aminobenzoate join together to form the construction of the hydrogen bond web. Two coordinated hydroxyl and two free water as well as two free chlorine anions form a six-membered ring (Supplementary Fig. 3s). O6 atom from free water molecule connects O5 atom in the six-membered ring and Cl2 anion, which links Mn(IV) ions to a 1D chain along *b*-axis (Fig. 8). N atoms of two 4-aminobenzoate join Cl1 anion to another 1D chain along *a*-axis, therefore complex **3** is connected to 2D net-like structure in *ab* plane (Supplementary Fig. 4s). Hydrogen bond data for complex **3** are given in Supplementary Table 1s and selected bond lengths and bond angles are also listed in Supplementary Table 2s.

3.2. SPS of complexes 1, 2 and 3

The surface photovoltage spectra were measured with a home-built apparatus described in Supplementary Figs. 5s and 6s in the range of 300–800 nm. A signal detected by SPS is equivalent to the change in the surface potential barrier on illumination (δV_s), which is given by the equation $\delta V_s = V_s - V_s^0$, where V_s^0 and V_s are the surface potential barriers before and after illumination, respectively [28]. The principles of SPS (Figs. 7s and 8s) and the analysis for spectral bands (Fig. 9s) are described in Supplementary material. The electrode is made of optical glass coated with indium and tin oxides (ITO). Standard p-typed silicon flake is used to adjust comparative phase and xenon lamp is used as an illuminant to supply a radiation in the range of 300–800 nm. The crystals are powdered and put into sample cell which is consisted of an ITO/sample/ITO sandwich structure. In order to make the light radiate the sample perpendicularly, the position of sample cell is adjusted and the surface photovoltage and external field induced surface

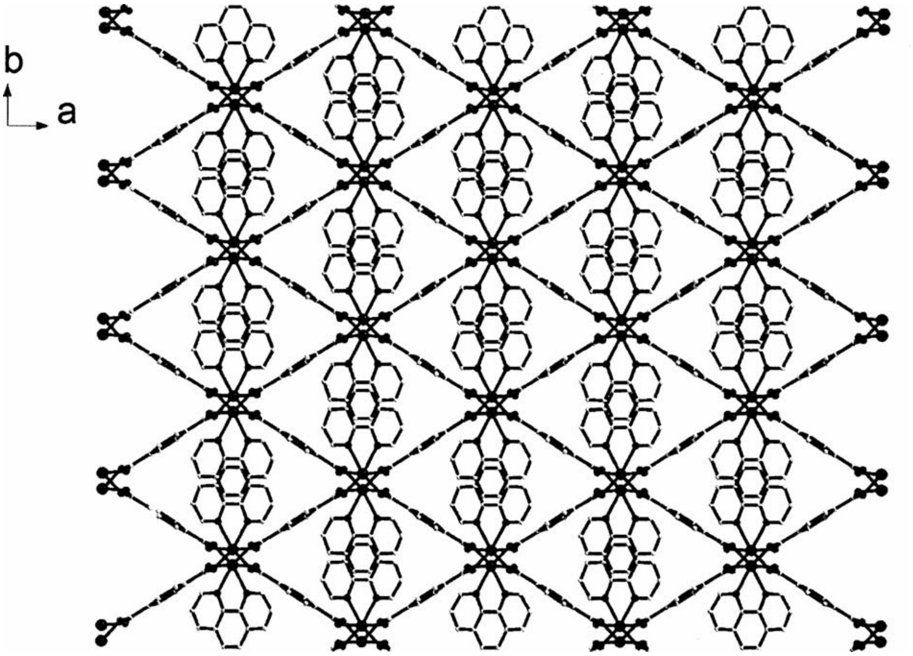

Fig. 4. The projection along *c*-axis of complex **1**.

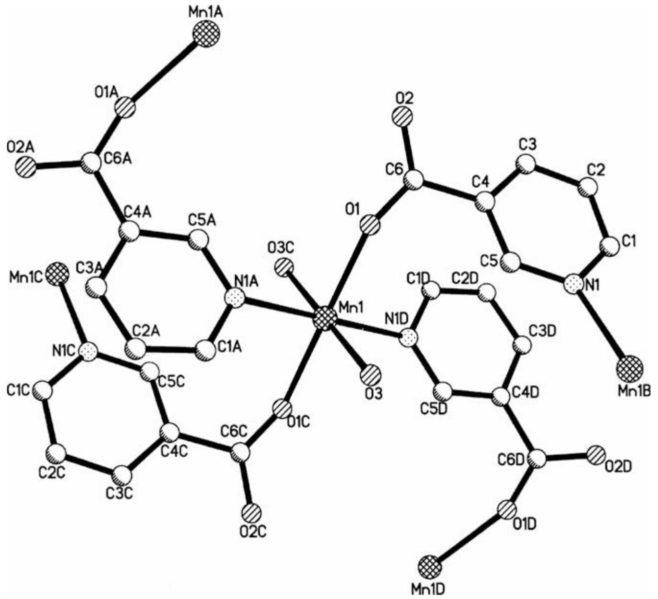

Fig. 5. Coordination environment of Mn(II) ion in complex **2**.

photovoltage under a discontinuous electric field have been measured.

Fig. 9 shows the SPS of complex **1** in which there is a wide and strong response band within 300–475 nm. After treated by program ORIGIN 7.0 [17], the response band can be divided into two positive responses. The response at $\lambda_{max} = 351$ nm is attributed to the $\pi \rightarrow \pi^*$ transition of ligands while the response at $\lambda_{max} = 383$ nm is assigned to the LMCT transition (from ligand to metal charge transfer transition). Meanwhile, there are some weak and splitting peaks in 475–550 nm, which are caused by $d \rightarrow d^*$ transition ($^6A_1 \rightarrow {}^4T_1$) of Mn(II, d^5) ion in a weaker crystal-field coordination environment.

The SPS of complex **2** (Fig. 10) shows a broad response band which seemed to be an overlap of three positive response bands in the range of 300–550 nm. The SPV response at $\lambda_{max} = 343$ nm is attributed to the $\pi \rightarrow \pi^*$ transition of ligands and the response at $\lambda_{max} = 375$ nm is assigned to the LMCT transition while the response at $\lambda_{max} = 429$ nm can be assigned to the $d \rightarrow d^*$ transition ($^2T_2 \rightarrow {}^2A_2$, $^2T_2$) of Mn(II) ion. Because the Mn(II) ion in complex **2** lies in a stronger crystal-field and the transitions of $^2T_2 \rightarrow {}^2A_2$, $^2T_2$ are allowed, the response at $\lambda_{max} = 429$ nm can be clearly observed.

In the SPS of complex **3** (Fig. 11), three positive response bands in 300–650 nm were observed. The SPV response with the higher energy can be divided into two bands: $\lambda_{max} = 334$ nm and $\lambda_{max} = 364$ nm. They can be attributed to $\pi \rightarrow \pi^*$ transition of ligands and LMCT, respectively. The two lower responses at $\lambda_{max} = 440$ nm and $\lambda_{max} = 557$ nm can be assigned to the $d \rightarrow d^*$ transitions of Mn(IV) ion ($^4A_2 \rightarrow {}^4T_1$ and $^4A_2 \rightarrow {}^4T_2$) in a stronger crystal-field. The SPS spectra of the three complexes are consistent with their UV–Vis spectra. The UV–Vis spectra of the three complexes are treated by ORIGIN 7.0 and displayed in Supplementary Figs. 10s, 11s and 12s. The analysis and contrast of SPS and UV–Vis spectroscopy of the three complexes are listed in Supplementary Table 3s.

Two differences are shown when we compared the SPS of complexes **1**–**3** (Fig. 12). First of all, the SPV intensity of complexes decreases gradually from **1–3**, mainly because of the different structure of the three complexes: Complex **1** possesses a 3D infinite structure which can supply more transmission passages for electrons or holes. More electrons diffuse to surface can lead an increase of SPV intensity. Meanwhile, the *ac* plane and *bc* plane in complex **1** are both regular, which is very favorable for transmitting electrons or holes. Complex **2** possesses an irregular 2D structure, which is less favorable for transferring electrons or holes than the regular one. So the SPV intensity of complex **1** is higher than that of complex **2**. Complex **3** is a mononuclear complex and the molecules are further connected to 2D structure by hydrogen bonds. So the SPV intensity of complex **3** is obviously lower than that of complexes **1** and **2**. Secondly, the position of $d \rightarrow d^*$ transition is obviously different, which can be attributed to the coordination environment and valences of manganese ions in the three complexes. As same as complex **1**, the six coordinated atoms of

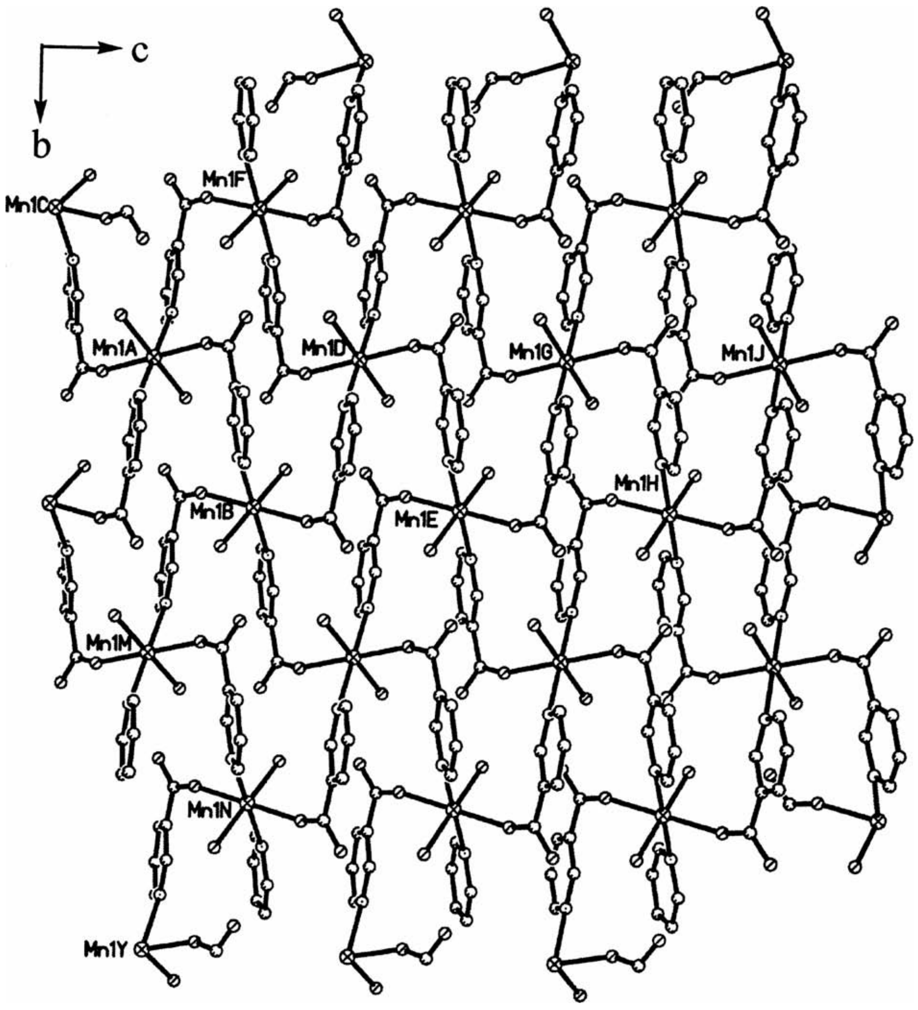

Fig. 6. The 2D infinite structure of complex **2**.

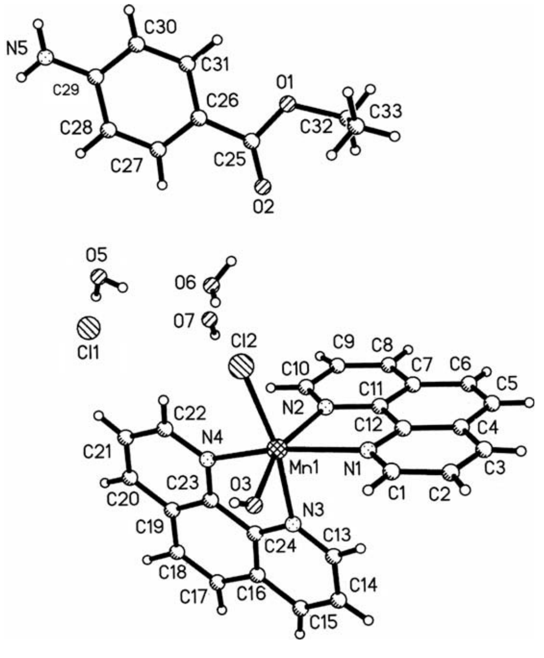

Fig. 7. Molecular structure of complex **3**.

Mn(II) ion are two N atoms and four O atoms in complex **2**. The difference between complexes **1** and **2** is that the four O atoms are all from carboxylic moieties in complex **1**, while only two O atoms are from carboxylic moieties and the other O atoms are from coordinated water molecules in complex **2**. According to the spectra chemical series (–COO < H_2O < N complexes), Mn(II, d^5) ion in complex **1** can be regarded as lying among a weaker crystal-field, so the $d \rightarrow d^*$ transition is forbidden. In complex **2**, Mn(II) ion is in a stronger octahedron field and the transitions of $^2T_2 \rightarrow {}^2A_2$ and $^2T_2 \rightarrow {}^2T_2$ are allowed, so the SPV response of $d \rightarrow d^*$ transition can be observed. In complex **3**, the valence of manganese ion is +4 and the coordinated atoms are four N atoms, one O atom and one Cl anion. The Mn(IV, d^3) ion is lying in a stronger field and the transitions of $^4A_2 \rightarrow {}^4T_1$ and $^4A_2 \rightarrow {}^4T_2$ are allowed, so it shows two obvious response bands of $d \rightarrow d^*$ transitions in the SPS.

*3.3. FISPS of complexes **1**, 2 and **3***

FISPS is a technique which combines the field effect principle with SPS. With a discontinuous d.c. electric field applying to both sides of the sample, the mobile direction and diffusive distance of photogenerated charge will vary, even the built-in field of the sample could change direction. If a positive electric field (the illuminated surface is positive) is applied vertically to the p-typed semiconductor surface, the separation efficiency of the photogeneration charge will enhance and the intensity of SPV response will

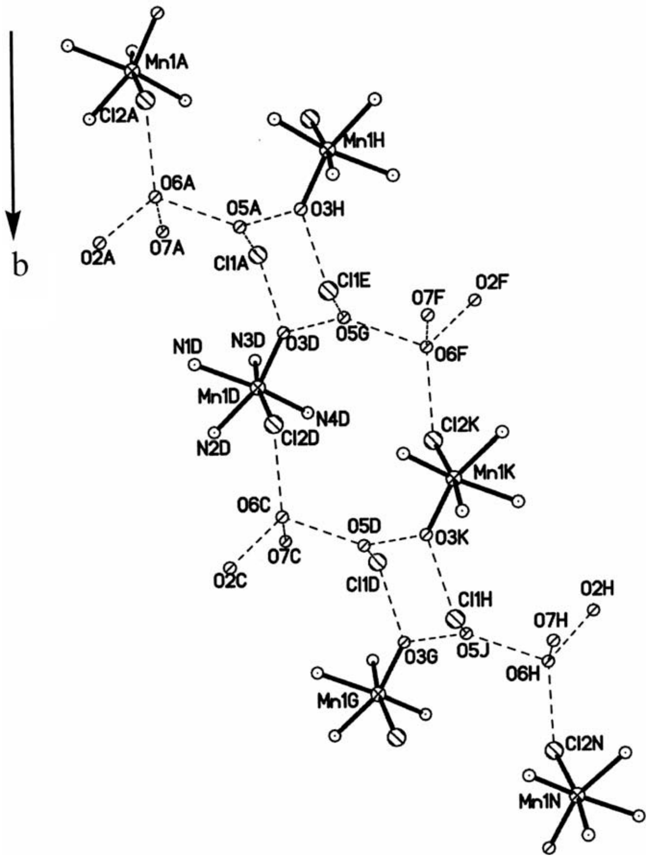

Fig. 8. Hydrogen bonds in *b*-axis of complex **3**.

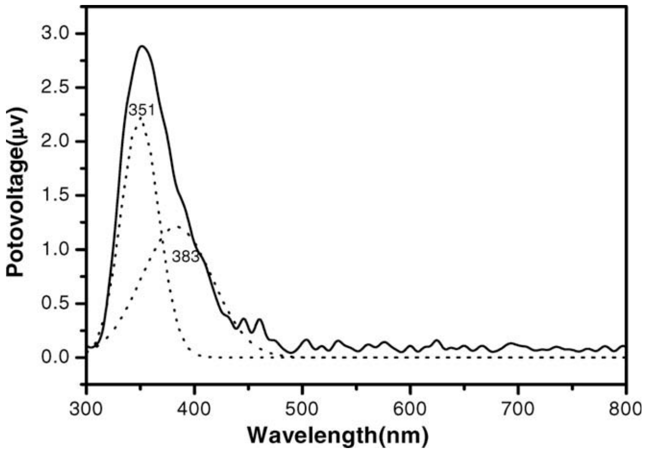

Fig. 9. SPS of complex **1** (dotted lines are peaks treated by ORIGIN 7.0).

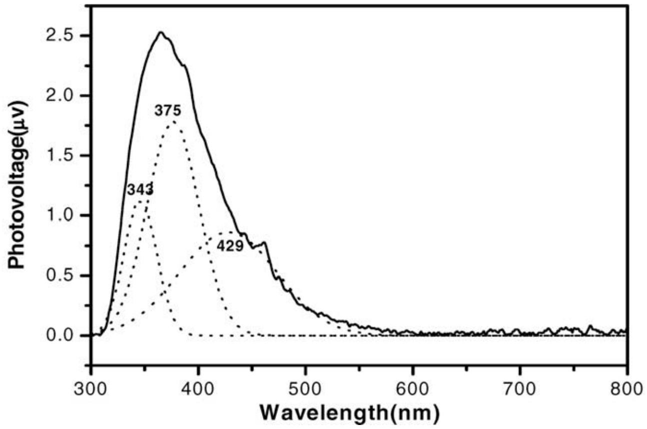

Fig. 10. SPS of complex **2** (dotted lines are peaks treated by ORIGIN 7.0).

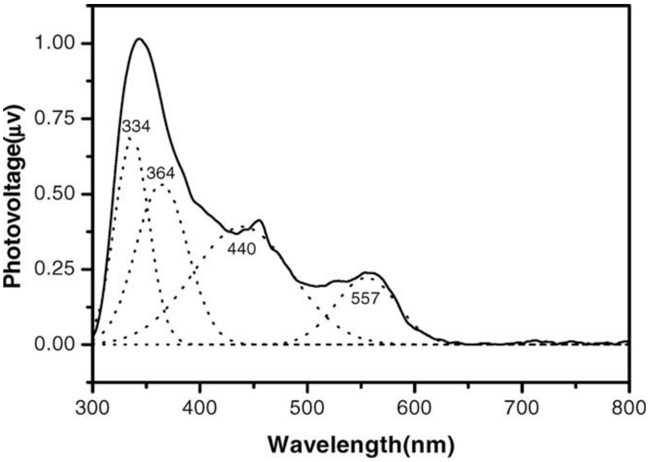

Fig. 11. SPS of complex **3** (dotted lines are peaks treated by ORIGIN 7.0).

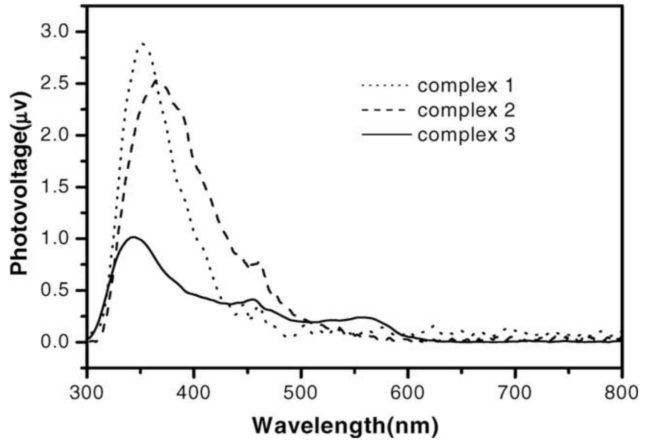

Fig. 12. The SPS contrast of the three complexes.

increase in the original direction. However, if a negative electric field in the opposite direction is applied to the built-in field, the separation efficiency of electrons and holes will reduce so that the intensity of SPV responses will weaken. With the aid of FISPS, the photo-induced charge transfer process can be detected and even some spectral characteristics can be interpreted. Fig. 13 is the FISPS of complex **2** when the external electric fields are −0.5 V, −1.0 V, +0.5 V and +1.0 V, respectively. The FISPS of complexes **1** and **3** (Supplementary Figs. 13s and 14s) are similar to that of complex **2**. The FISPS results indicate that the SPV response intensity increases linearly of all three complexes when the external positive fields increases; while reduces when the external negative fields increases. This is due to an external positive electric field is in favor of the separation of photo-excited electron–hole pairs, which in turn results in an increase of response intensity. A negative electric field has just the opposite effect.

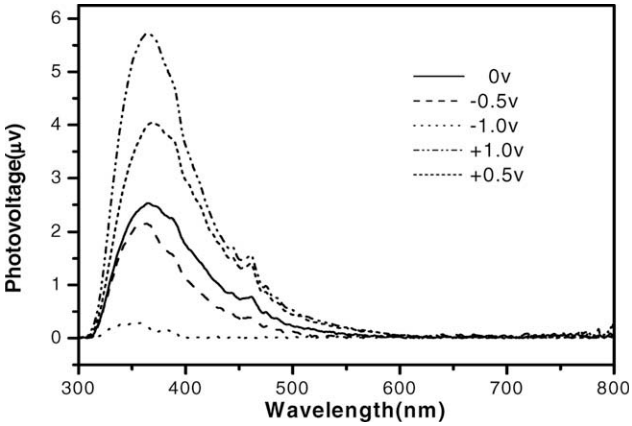

Fig. 13. FISPS of complex **2**.

4. Conclusion

In this study, the synthesis, analysis of crystal structures, full characterization and photoelectric property of three novel manganese complexes are presented. Complexes **1** and **2** are both coordination polymers possessing 3D and 2D infinite structures respectively. Complex **3** is a 2D coordination supramolecule connected by hydrogen bonds. The surface photovoltage spectra all show positive responses in the range 300–800 nm. But the intensity, position and numbers of the SPV response bands are apparently different from one another. The main reasons believed to be the differences in structure, valence and coordination sphere of manganese ions in the three complexes. First, the intensity of SPV bands is affected by the structures of the complexes. More dimensional structure can supply more transmission passages for electrons or holes which make the SPV intensity increase. Second, the valence of metal ion impacts the number of SPV bands. Third, the number and position of the SPV bands can be impacted by the coordinated environment of metal ions. When the metal ions are in different crystal fields or even the coordinated atoms are the only differences, it may trigger different transitions between the d orbitals of the metal ions, so the SPV response bands will exhibit noticeable differences.

Acknowledgements

This work was supported by the National Natural Science Foundation of China (Nos. 20571037 and 90201018) and the open fund of the State Key Laboratory of Rare Earth Material Chemistry and Application, Peking University of China.

Appendix A. Supplementary material

CCDC 638237, 638236 and 651307 contain the supplementary crystallographic data for **1**, **2** and **3**. These data can be obtained free of charge from The Cambridge Crystallographic Data Centre via www.ccdc.cam.ac.uk/data_request/cif. Supplementary data associated with this article can be found, in the online version, at doi:10.1016/j.ica.2008.07.010.

References

[1] P.J. Hagrman, D. Hagrman, J. Zubieta, Angew. Chem., Int. Ed. 38 (1999) 2638.
[2] T.K. Maji, S. Sain, G. Mostafa, T.H. Lu, J. Ribas, M. Monfort, N.R. Chaudhuri, Inorg. Chem. 42 (2003) 709.
[3] S. Feng, R. Xu, Acc. Chem. Res. 34 (2001) 239.
[4] (a) A. Tarushi, P. Christofis, G. Psomas, Polyhedron 26 (2007) 3963;
(b) A. Majumder, M. Westerhausen, A.N. Kneifel, J.P. Sutter, N. Daro, S. Mitra, Inorg. Chim. Acta 359 (2006) 3841.
[5] D. Maspoch, J.G. Segura, N. Domingo, D.R. Molina, K. Wurst, C. Rovira, J. Tejada, J. Veciana, Inorg. Chem. 44 (2005) 6936.
[6] (a) R.A. Lal, S. Bhaumik, A. Lemtur, M.K. Singh, D. Basumatari, S. Choudhury, A. De, A. Kumar, Inorg. Chim. Acta 359 (2006) 3105;
(b) M.L. Feng, H.Y. Ye, J.G. Mao, J. Solid State Chem. 180 (2007) 2471.
[7] S.V. Krivovichev, V. Kahlenberg, I.G. Tananaev, R. Kaindl, E. Mersdorf, B.F. Myasoedov, J. Am. Chem. Soc. 127 (2005) 1072.
[8] W. Dong, Q.L. Wang, S.F. Si, D.Z. Liao, Z.H. Jiang, S.P. Yan, P. Cheng, Inorg. Chem. Commun. 6 (2003) 873.
[9] T.M. Rajendiran, L.M. Kirk, I.A. Setyawati, Chem. Commun. 6 (2003) 824.
[10] Z. Shi, S. Feng, S. Gao, L. Zhang, G. Yang, J. Hua, Angew. Chem., Int. Ed. 39 (2000) 2325.
[11] W. Zhao, Y. Song, T. Okamura, J. Fan, W.Y. Sun, N. Ueyama, Inorg. Chem. 44 (2005) 3330.
[12] C.N.R. Rao, J.N. Behera, D. Meenakshi, Chem. Soc. Rev. 35 (2006) 375.
[13] Y.L. Wei, H.W. Hou, L. Li, Y.T. Fan, Y. Zhu, Cryst. Growth Des. 5 (2005) 1405.
[14] A. Pramanik, S. Abbina, G. Das, Polyhedron 26 (2007) 5225.
[15] A. Choudhury, D. Udayakumar, C.N.R. Rao, Angew. Chem., Int. Ed. 41 (2002) 158.
[16] U. Kortz, M.G. Savelieff, F.Y.A. Ghali, L.M. Khalil, S.A. Maalouf, D.I. Sinno, Angew. Chem., Int. Ed. 41 (2002) 4070.
[17] L.P. Sun, S.Y. Niu, J. Jin, G.D. Yang, L. Ye, Eur. J. Inorg. Chem. (2006) 5130.
[18] D.J. Wang, J. Zhang, T.S. Shi, B.H. Wang, X.Z. Cao, T.J. Li, J. Photochem. Photobiol. A: Chem. 93 (1996) 21.
[19] Y.H. Lin, D.J. Wang, Q.D. Zhao, M. Yang, Q.L. Zhang, J. Phys. Chem. B 108 (2004) 3202.
[20] J. Zhang, D.J. Wang, Y.M. Chen, T.J. Li, H.F. Mao, H.J. Tian, Q.F. Zhou, H.J. Xu, Thin Solid Films 300 (1997) 208.
[21] L. Kronik, Y. Shapira, Surf. Sci. Rep. 37 (1999) 1.
[22] F. Lenzmann, J. Krueger, S. Burnside, K. Brooks, M. Gratzel, D. Gal, S. Ruhle, D. Cahen, J. Phys. Chem. B 105 (2001) 6347.
[23] T.F. Xie, D.J. Wang, L.J. Zhu, T.J. Li, Y.J. Xu, Mater. Chem. Phys. 70 (2001) 103.
[24] M.H. Qi, G.F. Liu, J. Phys. Chem. B 107 (2003) 7640.
[25] J. Zhang, D.J. Wang, T.S. Shi, B.H. Wang, J.Z. Sun, T.J. Li, Thin Solid Films 284–285 (1996) 596.
[26] Q.L. Zhang, D.J. Wang, J.J. Xu, J. Cao, J.Z. Sun, M. Wang, Mater. Chem. Phys. 82 (2003) 525.
[27] Y.A. Cao, Q.J. Meng, W.S. Yang, J.H. Yao, Y.C. Shu, W. Wang, G.H. Chen, Colloids Surf. A 262 (2005) 181.
[28] V. Donchev, K. Kirilov, T. Ivanov, K. Germanova, Mater. Sci. Eng. B 129 (2006) 186.